A LARGER ESTIMATE OF THE ENTROPY OF THE UNIVERSE

Chas A. Egan[1,2] and Charles H. Lineweaver[3]

[1] Research School of Astronomy and Astrophysics, Australian National University, Canberra, Australia; chas@mso.anu.edu.au
[2] Department of Astrophysics, School of Physics, University of New South Wales, Sydney, Australia
[3] Planetary Science Institute, Research School of Astronomy and Astrophysics and Research School of Earth Sciences,
Australian National University, Canberra, Australia

ABSTRACT

Using recent measurements of the supermassive black hole (SMBH) mass function, we find that SMBHs are the largest contributor to the entropy of the observable universe, contributing at least an order of magnitude more entropy than previously estimated. The total entropy of the observable universe is correspondingly higher, and is $S_{\mathrm{obs}} = 3.1^{+3.0}_{-1.7} \times 10^{104}\,k$. We calculate the entropy of the current cosmic event horizon to be $S_{\mathrm{CEH}} = 2.6 \pm 0.3 \times 10^{122}\,k$, dwarfing the entropy of its interior, $S_{\mathrm{CEH\,int}} = 1.2^{+1.1}_{-0.7} \times 10^{103}\,k$. We make the first tentative estimate of the entropy of weakly interacting massive particle dark matter within the observable universe, $S_{\mathrm{dm}} = 10^{88\pm1}\,k$. We highlight several caveats pertaining to these estimates and make recommendations for future work.

Key words: black hole physics – cosmology: miscellaneous – diffusion – elementary particles – gravitation – neutrinos

Online-only material: color figures

1. INTRODUCTION

The entropy budget of the universe is important because its increase is associated with all irreversible processes, on all scales, across all facets of nature: gravitational clustering, accretion disks, supernovae, stellar fusion, terrestrial weather, and chemical, geological, and biological processes (Frautschi 1982; Lineweaver & Egan 2008).

Recently, Frampton et al. (2009) and Frampton & Kephart (2008) reported the entropy budget of the observable universe. Their budgets (listed beside others in Table 1) estimate the total entropy of the observable universe to be $S_{\mathrm{obs}} \sim 10^{102}\,k\text{–}10^{103}\,k$, dominated by the entropy of supermassive black holes (SMBHs) at the centers of galaxies. That the increase of entropy has not yet been capped by some limiting value, such as the holographic bound ('t Hooft 1993; Susskind 1995) at $S_{\mathrm{max}} \sim 10^{123}\,k$ (Frampton et al. 2009), is the reason dissipative processes are ongoing and that life can exist.

In this paper, we improve the entropy budget by using recent observational data and quantifying uncertainties. The paper is organized as follows. In what remains of the Introduction, we describe two different schemes for quantifying the increasing entropy of the universe, and we comment on caveats involving the identification of gravitational entropy. Our main work is presented in Sections 2 and 3, where we calculate new entropy budgets within each of the two accounting schemes. We finish in Section 4 with a discussion touching on the time evolution of the budgets we have calculated, and ideas for future work.

Throughout this paper, we assume flatness ($\Omega_k = 0$) as predicted by inflation (Guth 1981; Linde 1982) and supported by observations (Spergel et al. 2007). Adopted values for other cosmological parameters are $h = 0.705 \pm 0.013$, $\omega_b = \Omega_b h^2 = 0.0224 \pm 0.0007$, $\omega_m = \Omega_m h^2 = 0.136 \pm 0.003$ (Seljak et al. 2006), and $T_{\mathrm{CMB}} = 2.725 \pm 0.002$ K (Mather et al. 1999; quoted uncertainties are 1σ).

1.1. Two Schemes for Quantifying the Increasing Entropy of the Universe

Modulo statistical fluctuations, the generalized second law of thermodynamics holds that the entropy of the universe (including Bekenstein–Hawking entropy in the case of any region hidden behind an event horizon), must not decrease with time (Bekenstein 1974; Gibbons & Hawking 1977). Within the FRW framework, the generalized second law can be applied in at least two obvious ways.

1. The total entropy in a sufficiently large comoving volume of the universe does not decrease with cosmic time,

$$dS_{\mathrm{comoving\ volume}} \geqslant 0. \qquad (1)$$

2. The total entropy of matter contained within the cosmic event horizon (CEH) plus the entropy of the CEH itself, does not decrease with cosmic time,

$$dS_{\mathrm{CEH\ interior}} + dS_{\mathrm{CEH}} \geqslant 0. \qquad (2)$$

In the first of these schemes, the system is bounded by a closed comoving surface. The system is effectively isolated because large-scale homogeneity and isotropy imply no net flows of entropy into or out of the comoving volume. The time-slicing in this scheme is along surfaces of constant cosmic time. Event horizons of black holes are used to quantify the entropy of black holes; however, the CEH is neglected since the assumption of large-scale homogeneity makes it possible for us to keep track of the entropy of matter beyond it. A reasonable choice for the comoving volume in this scheme is the comoving sphere that presently corresponds to the observable universe, i.e., the gray area in Figure 1. Correspondingly, in Section 2 we calculate the present entropy budget of the observable universe and we do not include the CEH.

The second scheme is similar to the first in that we time-slice along surfaces of constant cosmic time. However, here
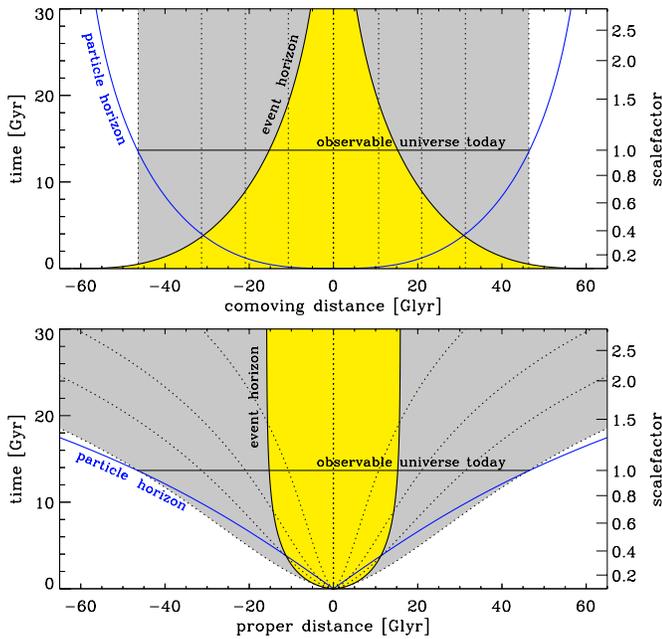
Figure 1. Panels show the particle horizon (see Equation (A1) and Figure 9) and the cosmic event horizon (see Equation (A5)) as a function of time. The difference between the two panels is the spatial coordinate system used: the x-axis in the bottom panel is proper distance D and in the top panel it is comoving distance $\chi \equiv \frac{D}{a}$, where a is the cosmic scalefactor. The origin is chosen so that our galaxy is the central vertical dotted line. The other dotted lines represent distant galaxies, which are approximately comoving and recede as the universe expands. The region inside the particle horizon is the observable universe. The comoving volume that corresponds to the observable universe today, about 13.7 Gyr after the big bang, is filled gray. In scheme 1, the entropy within this comoving volume increases (or remains constant) with time. Alternatively, in scheme 2 the entropy within the event horizon (the region filled yellow), plus the entropy of the horizon itself, increases (or remains constant) with time.

(A color version of this figure is available in the online journal.)

the system (yellow shade in Figure 1) is bounded by the time-dependent CEH instead of a comoving boundary. Migration of matter across the CEH is not negligible, and the CEH entropy (Gibbons & Hawking 1977) must be included in the budget to account for this (e.g., Davis et al. 2003). The present entropy of the CEH and its interior is calculated in Section 3.

1.2. Entropy and Gravity

It is widely appreciated that non-gravitating systems of particles evolve toward homogenous temperature and density distributions. The corresponding increase in the volume of momentum-space and position-space occupied by the constituent particles represents an increase in entropy. On the other hand, strongly gravitating systems become increasingly lumpy. With "lumpyness" naively akin to "orderliness," it is not as easy to see that the total entropy increases. In these systems, the entropy is shared among numerous components, all of which must be considered.

For example, approximately collisionless long-range gravitational interactions between stars result in dynamical relaxation of galaxies (Lynden-Bell 1967; whereby bulk motions are dissipated and entropy is transferred to stars in the outer regions of the galaxy) and stellar evaporation from galaxies (whereby stars are ejected altogether, carrying with them energy, angular momentum, and entropy, and allowing what remains behind to contract; e.g., Binney & Tremaine 2008). In more highly dissipative systems, i.e., accretion disks, non-gravitational interac-

tions (viscosity and/or magnetorotational instability; Balbus & Hawley 2002) transfer angular momentum and dissipate energy and entropy.

In addition to these considerations, entropy also increases when gravitons are produced. A good example is the in-spiral of close binaries, such as the Hulse–Taylor binary pulsar system (Hulse & Taylor 1975; Weisberg & Taylor 2005). Gravitational waves emitted from the system extract orbital energy (and therefore entropy) allowing the system to contract.

The entropy of a general gravitational field is still not known. Penrose (1987, 1979, 2004) has proposed that it is related to the Weyl curvature tensor $W_{\mu\nu\kappa\lambda}$. In conformally flat spacetimes (such as an ideal FRW universe), the Weyl curvature vanishes and gravitational entropy is postulated to vanish (to limits imposed by quantum uncertainty). In clumpy spacetimes, the Weyl curvature takes large values and the gravitational entropy is high. While Ricci curvature $R_{\mu\nu}$ vanishes in the absence of matter, Weyl curvature may still be non-zero (e.g., gravitational waves traveling though empty space) and the corresponding gravitational entropy may be non-zero.

If these ideas are correct then the low gravitational entropy of the early universe comes from small primordial gravitational perturbations. Gravitational entropy then increases with the growing amplitude of linear density fluctuations parameterized through the matter power spectrum $P(k)$. The present gravitational entropy, however, is expected to be dominated by the nonlinear overdensities (with large Weyl tensors) which have formed since matter-radiation equality.

In extreme cases, gravitational clumping leads to the formation of black holes. The entropy of black holes is well known (Bekenstein 1973; Hawking 1976; Strominger & Vafa 1996). The entropy of a Schwarzschild black hole is given by

$$S_{\mathrm{BH}} = \frac{kc^3}{G\hbar}\frac{A}{4} = \frac{4\pi kG}{c\hbar}M^2, \qquad (3)$$

where $A = \frac{16\pi G^2 M^2}{c^4}$ is the event-horizon area and M is the black hole mass.

Because gravitational entropy is difficult to quantify, we only include it in the two extremes: the thermal distribution of gravitons and black holes.

2. THE PRESENT ENTROPY OF THE OBSERVABLE UNIVERSE

The present entropy budget of the observable universe was estimated most recently by Frampton et al. (2009) and Frampton & Kephart (2008). These papers and earlier work (Kolb & Turner 1981; Frautschi 1982; Penrose 2004; Bousso et al. 2007) identified the largest contributors to the entropy of the observable universe as black holes, followed distantly by the cosmic microwave background (CMB) and the neutrino background. The last column of Table 1 contains previous estimates of the entropy in black holes, the CMB and neutrinos, as well as several less significant components.

Sections 2.1–2.7 below describe the data and assumptions used to calculate our entropy densities (given in Column 2 of Table 1). Our entropy budget for the observable universe (Column 3 of Table 1) is then found by multiplying the entropy density by the volume of the observable universe V_{obs},

$$S_i = s_i V_{\mathrm{obs}}, \qquad (4)$$

where s_i is the entropy density of component i. The volume of the observable universe is (see the Appendix)

$$V_{\rm obs} = 43.2 \pm 1.2 \times 10^4 \, {\rm Glyr}^3$$
$$= 3.65 \pm 0.10 \times 10^{80} \, {\rm m}^3. \quad (5)$$

2.1. Baryons

For a non-relativistic, non-degenerate gas, the specific entropy (entropy per baryon) is given by the Sakur–Tetrode equation (e.g., Basu & Lynden-Bell 1990)

$$(s/n_b) = \frac{k}{n_b} \sum_i n_i \ln \left[Z_i(T)(2\pi m_i kT)^{\frac{3}{2}} e^{\frac{5}{2}} n_i^{-1} h^{-3} \right], \quad (6)$$

where i indexes particle types in the gas, n_i is the ith particle type's number density, and $Z_i(T)$ is its internal partition function. Basu & Lynden-Bell (1990) found specific entropies between $11\,k$ and $21\,k$ per baryon for main-sequence stars of approximately solar mass. For components of the interstellar medium (ISM) and intergalactic medium (IGM), they found specific entropies between $20\,k$ (H_2 in the ISM) and $143\,k$ (ionized hydrogen in the IGM) per baryon.

The cosmic entropy density in stars s_* can be estimated by multiplying the specific entropy of stellar material by the cosmic number density of baryons in stars n_{b*}:

$$s_* = (s/n_b)_* n_{b*} = (s/n_b)_* \frac{\rho_*}{m_p} = (s/n_b)_* \left[\frac{3H^2}{8\pi G} \frac{\Omega_*}{m_p} \right]. \quad (7)$$

Using the stellar cosmic density parameter $\Omega_* = 0.0027 \pm 0.0005$ (Fukugita & Peebles 2004) and the range of specific entropies for main-sequence stars around the solar mass (which dominate stellar mass), we find

$$s_* = 0.26 \pm 0.12 \, k \, {\rm m}^{-3}, \quad (8)$$

$$S_* = 9.5 \pm 4.5 \times 10^{80} \, k. \quad (9)$$

Similarly, the combined energy density for the ISM and IGM is $\Omega_{\rm gas} = 0.040 \pm 0.003$ (Fukugita & Peebles 2004), and by using the range of specific entropies for ISM and IGM components, we find

$$s_{\rm gas} = 20 \pm 15 \, k \, {\rm m}^{-3}, \quad (10)$$

$$S_{\rm gas} = 7.1 \pm 5.6 \times 10^{81} \, k. \quad (11)$$

The uncertainties in Equations (9) and (11) are dominated by uncertainties in the mass weighting of the specific entropies, but also include uncertainties in Ω_*, $\Omega_{\rm gas}$, and the volume of the observable universe.

2.2. Photons

The CMB photons are the most significant non-black hole contributors to the entropy of the observable universe. The distribution of CMB photons is thermal (Mather et al. 1994) with a present temperature of $T_\gamma = 2.725 \pm 0.002 \, {\rm K}$ (Mather et al. 1999).

The entropy of the CMB is calculated using the equation for a black body (e.g., Kolb & Turner 1990),

$$s_\gamma = \frac{2\pi^2}{45} \frac{k^4}{c^3 \hbar^3} g_\gamma T_\gamma^3$$
$$= 1.478 \pm 0.003 \times 10^9 \, k \, {\rm m}^{-3}, \quad (12)$$

$$S_\gamma = 2.03 \pm 0.15 \times 10^{89} \, k, \quad (13)$$

where $g_\gamma = 2$ is the number of photon spin states. The uncertainty in Equation (13) is dominated by uncertainty in the size of the observable universe.

The non-CMB photon contribution to the entropy budget (including starlight and heat emitted by the ISM) is somewhat less, at around $10^{86} \, k$ (Frautschi 1982; Bousso et al. 2007; Frampton et al. 2009).

2.3. Relic Neutrinos

The neutrino entropy cannot be calculated directly since the temperature of cosmic neutrinos has not been measured. Standard treaties of the radiation era (e.g., Kolb & Turner 1990; Peacock 1999) describe how the present temperature (and entropy) of massless relic neutrinos can be calculated from the well-known CMB photon temperature. Since this background physics is required for Sections 2.4 and 2.5, we summarize it briefly here.

A simplifying feature of the radiation era (at least at known energies $\lesssim 10^{12}$ eV) is that the radiation fluid evolves adiabatically: the entropy density decreases as the cube of the increasing scalefactor, $s_{\rm rad} \propto a^{-3}$. The evolution is adiabatic because reaction rates in the fluid are faster than the expansion rate H of the universe. It is convenient to write the entropy density as

$$s_{\rm rad} = \frac{2\pi^2}{45} \frac{k^4}{c^3 \hbar^3} g_{*S} T_\gamma^3 \propto a^{-3}, \quad (14)$$

where g_{*S} is the number of relativistic degrees of freedom in the fluid (with $m < kT/c^2$) given approximately by

$$g_{*S}(T) \approx \sum_{{\rm bosons},\, i} g_i \left(\frac{T_i}{T_\gamma} \right)^3 + \sum_{{\rm fermions},\, j} \frac{7}{8} g_j \left(\frac{T_j}{T_\gamma} \right)^3. \quad (15)$$

For photons alone, $g_{*S} = g_\gamma = 2$, and thus Equation (14) becomes Equation (12). For photons coupled to an electron–positron component, such as existed before electron–positron annihilation, $g_{*S} = g_\gamma + \frac{7}{8} g_{e\pm} = 2 + \frac{7}{8} 4 = \frac{11}{2}$.

As the universe expands, massive particles annihilate, heating the remaining fluid. The effect on the photon temperature is quantified by inverting Equation (14),

$$T_\gamma \propto a^{-1} g_{*S}^{-1/3}. \quad (16)$$

The photon temperature decreases less quickly than a^{-1} because g_{*S} decreases with time. Before electron–positron $e^\pm$ annihilation, the temperature of the photons was the same as that of the almost completely decoupled neutrinos. After $e^\pm$ annihilation heats only the photons, the two temperatures differ by a factor C,

$$T_\nu = C \, T_\gamma. \quad (17)$$

A reasonable approximation, $C \approx (4/11)^{1/3}$, is derived by assuming that only photons were heated during $e^\pm$ annihilation,

where 4/11 is the ratio of g_{*S} for photons to g_{*S} for photons, electrons, and positrons.

Corrections are necessary at the 10^{-3} level because neutrinos had not completely decoupled at $e^{\pm}$ annihilation (Gnedin & Gnedin 1998). The neutrino entropy density is computed assuming a thermal distribution with $T_{\nu} = (4/11)^{1/3}T_{\gamma}$, and we assign a 1% uncertainty.

$$s_{\nu} = \frac{2\pi^2}{45}\frac{k^4}{c^3\hbar^3}g_{\nu}\left(\frac{7}{8}\right)T_{\nu}^3$$
$$= 1.411 \pm 0.014 \times 10^9 \, k \text{ m}^{-3}, \qquad (18)$$

where $g_{\nu} = 6$ (3 flavors, 2 spin states each). The total neutrino entropy in the observable universe is then

$$S_{\nu} = 5.16 \pm 0.14 \times 10^{89} \, k \qquad (19)$$

with an uncertainty dominated by uncertainty in the volume of the observable universe.

Neutrino oscillation experiments have demonstrated that neutrinos are massive by measuring differences between the three neutrino mass eigenstates (Cleveland et al. 1998; Adamson et al. 2008; Abe et al. 2008). At least two of the mass eigenstates are heavier than ~ 0.009 eV. Since this is heavier than their current relativistic energy ($\frac{k}{2}CT_{\gamma} = 0.0001$ eV; computed under the assumption that they are massless) at least two of the three masses are presently non-relativistic.

Expansion causes non-relativistic species to cool as a^{-2} instead of a^{-1}, which would result in a lower temperature for the neutrino background than suggested by Equation (17). The entropy density (calculated in Equation (18)) and entropy (calculated in Equation (19)) are unaffected by the transition to non-relativistic cooling since the cosmic expansion of relativistic and non-relativistic gases are both adiabatic processes (the comoving entropy is conserved, so in either case $s \propto a^{-3}$).

We neglect a possible increase in neutrino entropy due to their infall into gravitational potentials during structure formation. If large, this will need to be considered in future work.

2.4. Relic Gravitons

A thermal background of gravitons is expected to exist, which decoupled from the photon bath around the Planck time, and has been cooling as $T_{\text{grav}} \propto a^{-1}$ since then. The photons cooled less quickly because they were heated by the annihilation of heavy particle species (Equation (16)). Thus, we can relate the current graviton temperature to the current photon temperature

$$T_{\text{grav}} = \left(\frac{g_{*S}(t_0)}{g_{*S}(t_{\text{planck}})}\right)^{1/3}T_{\gamma}, \qquad (20)$$

where $g_{*S}(t_{\text{planck}})$ is the number of relativistic degrees of freedom at the Planck time and $g_{*S}(t_0) = 3.91$ today (this is appropriate even in the case of massive neutrinos because they decoupled from the photon bath while they were still relativistic). Given the temperature of background gravitons, their entropy can be calculated as

$$s_{\text{grav}} = \frac{2\pi^2}{45}\frac{k^4}{c^3\hbar^3}g_{\text{grav}}T_{\text{grav}}^3, \qquad (21)$$

where $g_{\text{grav}} = 2$.

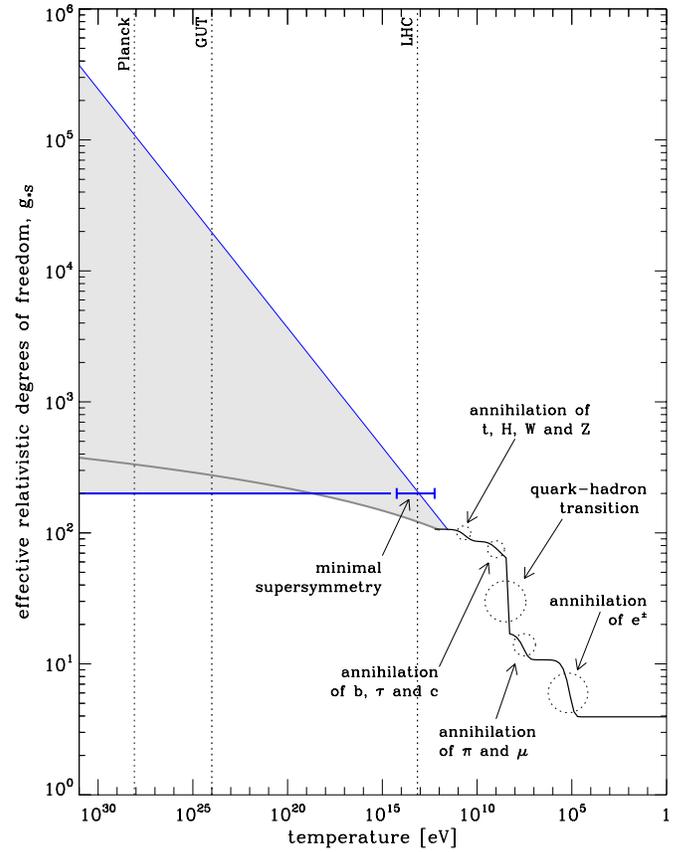Figure 2 shows g_{*S} as a function of temperature. The function is well known for temperatures below about 10^{12} eV,

Figure 2. Number of relativistic degrees of freedom g_{*S} as a function of temperature, computed using the prescription given by Coleman & Roos (2003). All the particles of the standard model are relativistic at $T \gtrsim 10^{12}$ eV and $g_{*S}(10^{12} \text{ eV}) = 106.75$. The value of g_{*S} is not known above $T \sim 10^{12}$. To estimate plausible ranges of values, we extrapolate g_{*S} linearly (gray line) and exponentially (thin blue line) in $\log(T)$. The minimum contribution to g_{*S} from supersymmetric partners is shown (blue bar) and taken to indicate a minimum likely value of g_{*S} at higher temperatures (thick blue line).

(A color version of this figure is available in the online journal.)

but is not known at higher temperatures. Previous estimates of the background graviton entropy have assumed $g_{*S}(t_{\text{planck}}) \sim g_{*S}(10^{12} \text{ eV}) = 106.75$ (Frampton et al. 2009; Frampton & Kephart 2008), but this should be taken as a lower bound on $g_{*S}(t_{\text{planck}})$ yielding an upper bound on T_{grav} and s_{grav}.

To get a better idea of the range of possible graviton temperatures and entropies, we have adopted three values for $g_{*S}(t_{\text{planck}})$. As a minimum likely value, we use $g_{*S} = 200$ (Figure 2, thick blue line), which includes the minimal set of additional particles suggested by supersymmetry. As our middle value we use $g_{*S} = 350$, corresponding to the linear extrapolation of g_{*S} in $\log(T)$ to the Planck scale (Figure 2, gray line). And as a maximum likely value we use $g_{*S} = 10^5$, corresponding to an exponential extrapolation (Figure 2, thin blue line).

The corresponding graviton temperatures today are (Equation (20))

$$T_{\text{grav}} = 0.61^{+0.12}_{-0.52} \text{ K}. \qquad (22)$$

Inserting this into Equation (21), we find the entropy in the relic graviton background to be

$$s_{\text{grav}} = 1.7 \times 10^{7^{+0.2}_{-2.5}} \, k \, \text{m}^{-3}, \tag{23}$$

$$S_{\text{grav}} = 6.2 \times 10^{87^{+0.2}_{-2.5}} \, k. \tag{24}$$

It is interesting to note the possibility of applying Equation (20) in reverse, i.e., calculating the number of relativistic degrees of freedom at the Planck time using future measurements of the graviton background temperature.

2.5. Dark Matter

The most compelling interpretation of dark matter is as a weakly interacting superpartner (or weakly interacting massive particle, WIMP). According to this idea, dark matter particles decoupled from the radiation background at some energy above the particle mass.

If this interpretation is correct, the fraction of relativistic background entropy in dark matter at the time dark matter decoupled $t_{\text{dm dec}}$ is determined by the fraction of relativistic degrees of freedom that were associated with dark matter at that time (see Equation (14)),

$$s_{\text{dm}} = \frac{g_{*S \text{ dm}}(t_{\text{dm dec}})}{g_{*S \text{ non-dm}}(t_{\text{dm dec}})} s_{\text{non-dm rad}}. \tag{25}$$

This can be evaluated at dark matter decoupling, or any time thereafter, since both s_{dm} and $s_{\text{non-dm rad}}$ are adiabatic ($\propto a^{-3}$).

We are unaware of any constraint on the number of superpartners that may collectively constitute dark matter. The requirements that they are only weakly interacting, and that they decouple at a temperature above their mass, are probably only satisfied by a few (even one) species. Based on these arguments, we assume $g_{*S \text{ dm}}(t_{\text{dm dec}}) \lesssim 20$ and $g_{*S}(t_{\text{dm dec}}) \gtrsim 106.75$ which yields the upper limit

$$\frac{g_{*S \text{ dm}}(t_{\text{dm dec}})}{g_{*S}(t_{\text{dm dec}})} \lesssim \frac{1}{5}. \tag{26}$$

On the other hand, there may be many more degrees of freedom than suggested by minimal supersymmetry. By extrapolating g_{*S} exponentially beyond supersymmetric scales (to 10^{15} eV), we find $g_{*S}(t_{\text{dm dec}}) \lesssim 800$. In the simplest case, dark matter is a single scalar particle so $g_{*S \text{ dm}}(t_{\text{dm dec}}) \gtrsim 1$ and we take as a lower limit

$$\frac{g_{*S \text{ dm}}(t_{\text{dm dec}})}{g_{*S \text{ non-dm}}(t_{\text{dm dec}})} \gtrsim \frac{1}{800}. \tag{27}$$

Inserting this into Equation (25) at the present day gives

$$s_{\text{dm}} = 5 \times 10^{7 \pm 1} \, k \, \text{m}^{-3}, \tag{28}$$

where we have used the estimated limits given in Equations (26) and (27) and taken $s_{\text{non-dm rad}}$ to be the combined entropy of neutrinos and radiation today (Equations (12) and (18)). The corresponding estimate for the total dark matter entropy in the observable universe is

$$S_{\text{dm}} = 2 \times 10^{88 \pm 1} \, k. \tag{29}$$

As with our calculated neutrino entropy, our estimates here carry the caveat that we have not considered changes in the dark matter entropy associated with gravitational structure formation.
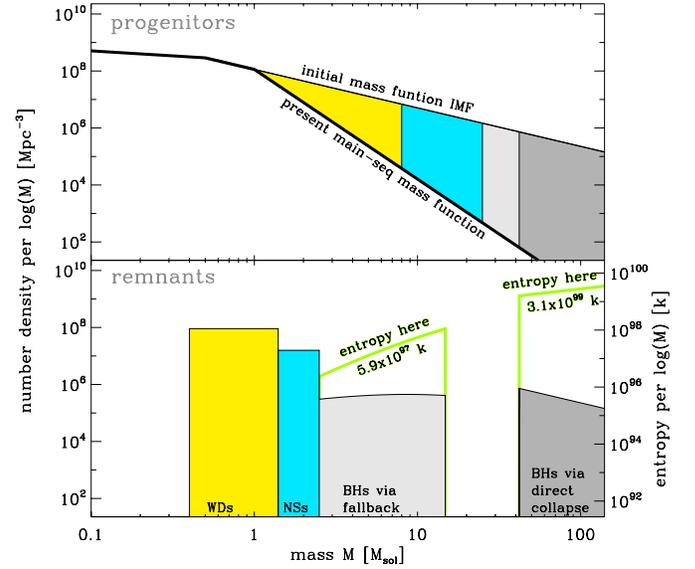

Figure 3. Progenitors in the IMF (top panel) evolve into the distribution of remnants in the bottom panel. The shape of the present main-sequence mass function differs from that of the IMF (top panel) by the stars that have died leaving white dwarfs (yellow), neutron stars (blue), and black holes (light and dark gray). The present distribution of remnants is shown in the bottom panel. Black holes in the range $2.5 \, M_\odot \lesssim M \lesssim 15 \, M_\odot$ (light gray) have been observationally confirmed. They form from progenitors in the range $25 \, M_\odot \lesssim M \sim 42 \, M_\odot$ via core collapse supernova and fallback, and we calculate their entropy to be $5.9 \times 10^{97^{+0.6}_{-1.2}} \, k$. Progenitors above about $42 \, M_\odot$, may evolve directly to black holes without significant loss of mass (dark gray) and may carry much more entropy, but this population has not been observed. The green curve, whose axis is on the right, shows the mass distribution of stellar black hole entropies in the observable universe.

(A color version of this figure is available in the online journal.)

2.6. Stellar Black Holes

In the top panel of Figure 3, we show the stellar initial mass function (IMF) parameterized by

$$\frac{dn_{\text{initial}}}{d \log M} \propto \left(\frac{M}{M_\odot} \right)^{\alpha+1}, \tag{30}$$

with $\alpha = -1.35$ at $M < 0.5 \, M_\odot$ and $\alpha = -2.35^{+0.65}_{-0.35}$ at $M \geqslant 0.5 \, M_\odot$ (Elmegreen 2007). We also show the present distribution of main-sequence stars, which is proportional to the initial distribution for $M \lesssim 1 \, M_\odot$, but which is reduced by a factor of $(M/M_\odot)^{-2.5}$ for heavier stars (Fukugita & Peebles 2004),

$$\frac{dn_{\text{present}}}{d \log(M)} = \begin{cases} \frac{dn_{\text{initial}}}{d \log(M)}, & \text{for } M < 1 \, M_\odot \\ \frac{dn_{\text{initial}}}{d \log(M)} \left(\frac{M}{M_\odot} \right)^{-2.5}, & \text{for } M \geqslant 1 \, M_\odot \end{cases}. \tag{31}$$

The initial and present distributions are normalized using the present cosmic density of stars, $\Omega_* = 0.0027 \pm 0.0005$ (Fukugita & Peebles 2004).

The yellow fill in the top panel represents stars of mass $1 \, M_\odot \lesssim M \lesssim 8 \, M_\odot$, which died leaving white dwarf remnants of mass $M \lesssim 1.4 \, M_\odot$ (yellow fill, bottom panel). The blue fill represents stars of mass $8 \, M_\odot \lesssim M \lesssim 25 \, M_\odot$, which died and left neutron star remnants of mass $1.4 \, M_\odot \lesssim M \lesssim 2.5 \, M_\odot$. The light gray area represents stars of mass $25 \, M_\odot \lesssim M \lesssim 42 \, M_\odot$, which became black holes of mass $2.5 \, M_\odot \lesssim M \lesssim 15 \, M_\odot$ via supernovae (here we use the simplistic final-initial mass function

Component	Entropy Density s (k m^{-3})	Entropy S (k)	Entropy S (k) (Previous Work)
SMBHs	$8.4^{+8.2}_{-4.7} \times 10^{23}$	$3.1^{+3.0}_{-1.7} \times 10^{104}$	10^{101}[1], 10^{102}[2], 10^{103}[3]
Stellar BHs (2.5–15 $M_\odot$)	$1.6 \times 10^{17^{+0.6}_{-1.2}}$	$5.9 \times 10^{97^{+0.6}_{-1.2}}$	10^{97}[2], 10^{98}[4]
Photons	$1.478 \pm 0.003 \times 10^9$	$5.40 \pm 0.15 \times 10^{89}$	10^{88}[1, 2, 4], 10^{89}[5]
Relic Neutrinos	$1.411 \pm 0.014 \times 10^9$	$5.16 \pm 0.15 \times 10^{89}$	10^{88}[2], 10^{89}[5]
WIMP Dark Matter	$5 \times 10^{7\pm1}$	$2 \times 10^{88\pm1}$	$\ldots$
Relic Gravitons	$1.7 \times 10^{7^{+0.2}_{-2.5}}$	$6.2 \times 10^{87^{+0.2}_{-2.5}}$	10^{86}[2, 3]
ISM and IGM	20 ± 15	$7.1 \pm 5.6 \times 10^{81}$	$\ldots$
Stars	0.26 ± 0.12	$9.5 \pm 4.5 \times 10^{80}$	10^{79}[2]
Total	$8.4^{+8.2}_{-4.7} \times 10^{23}$	$3.1^{+3.0}_{-1.7} \times 10^{104}$	10^{101}[1], 10^{102}[2], 10^{103}[3]
Tentative Components:			
Massive Halo BHs ($10^5\,M_\odot$)	10^{25}	10^{106}	10^{106}[6]
Stellar BHs (42–140 $M_\odot$)	$8.5 \times 10^{18^{+0.8}_{-1.6}}$	$3.1 \times 10^{99^{+0.8}_{-1.6}}$	$\ldots$

Notes. Our budget is consistent with previous estimates from the literature with the exception that SMBHs, which dominate the budget, contain at least an order of magnitude more entropy as previously estimated, due to the contributions of black holes 100 times larger than those considered in previous budgets. Uncertainty in the volume of the observable universe (see the Appendix) has been included in the quoted uncertainties. Massive halo black holes at $10^5\,M_\odot$ and stellar black holes in the range 42–140 $M_\odot$ are included tentatively since their existence is speculative. They are not counted in the budget totals. Previous work: (1) Penrose 2004, (2) Frampton et al. 2009, (3) Frampton & Kephart 2008, (4) Frautschi 1982, (5) Kolb & Turner 1981, (6) Frampton 2009b.

of Fryer & Kalogera (2001)). Stars larger than $\sim 42\,M_\odot$ collapse directly to black holes, without supernovae, and therefore retain most of their mass (dark gray regions; Fryer & Kalogera 2001; Heger et al. 2005).

Integrating Equation (3) over stellar black holes in the range $M \leqslant 15\,M_\odot$ (the light gray fill in the bottom panel of Figure 3), we find

$$s_{\text{SBH (M<15 M}_\odot)} = 1.6 \times 10^{17^{+0.6}_{-1.2}}\, k\ \text{m}^{-3}, \qquad (32)$$

$$S_{\text{SBH (M<15 M}_\odot)} = 5.9 \times 10^{97^{+0.6}_{-1.2}}\, k, \qquad (33)$$

which is comparable to previous estimates of the stellar black hole entropy (see Table 1). Our uncertainty is dominated by uncertainty in the slope of the IMF, but also includes uncertainty in the normalization of the mass functions and uncertainty in the volume of the observable universe.

If the IMF extends beyond $M \gtrsim 42\,M_\odot$ as in Figure 3, then these higher mass black holes (the dark gray fill in the bottom panel of Figure 3) may contain more entropy than black holes of mass $M < 15\,M_\odot$ (Equation (32)). For example, if the Salpeter IMF is reliable to $M = 140\,M_\odot$ (the Eddington limit and the edge of Figure 3), then black holes in the mass range 42–140 $M_\odot$ would contribute about $3.1 \times 10^{99^{+0.8}_{-1.6}}\, k$ to the entropy of the observable universe. Significantly less is known about this potential population, and should be considered a tentative contribution in Table 1.

2.7. Supermassive Black Holes

Previous estimates of the SMBH entropy (Penrose 2004; Frampton et al. 2009; Frampton & Kephart 2008) have assumed a typical SMBH mass and a number density and yield $S_{\text{SMBH}} = 10^{101}$–$10^{103}\, k$. Below we use the SMBH mass function as measured recently by Graham et al. (2007). Assuming a three-parameter Schechter function

$$\frac{dn}{d\log M} = \phi_* \left(\frac{M}{M_*}\right)^{\alpha+1} \exp\left[1 - \left(\frac{M}{M_*}\right)\right], \qquad (34)$$
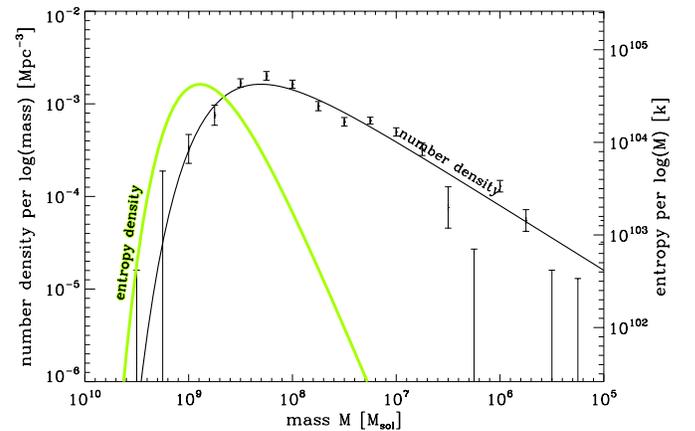

Figure 4. The entropy of supermassive black holes. The black curve, whose axis is on the left, is the SMBH mass function from Graham et al. (2007), i.e., the number of supermassive black holes per Mpc^3 per logarithmic mass interval. The green curve, whose axis is on the right, shows the mass distribution of SMBH entropies in the observable universe.

(A color version of this figure is available in the online journal.)

(number density per logarithmic mass interval) they find $\phi_* = 0.0016 \pm 0.0004$ Mpc^{-3}, $M_* = 2.9 \pm 0.7 \times 10^8\,M_\odot$, and $\alpha = -0.30 \pm 0.04$. The data and best-fit model are shown in black in Figure 4.

We calculate the SMBH entropy density by integrating Equation (3) over the SMBH mass function,

$$s = \frac{4\pi kG}{c\hbar} \int M^2 \left(\frac{dn}{d\log(M)}\right) d\log M. \qquad (35)$$

The integrand is plotted using a green line in Figure 4 showing that the contributions to SMBH entropy are primarily due to black holes around $\sim 10^9\,M_\odot$. The SMBH entropy is found to be

$$s_{\text{SMBH}} = 8.4^{+8.2}_{-4.7} \times 10^{23}\, k\ \text{m}^{-3}, \qquad (36)$$

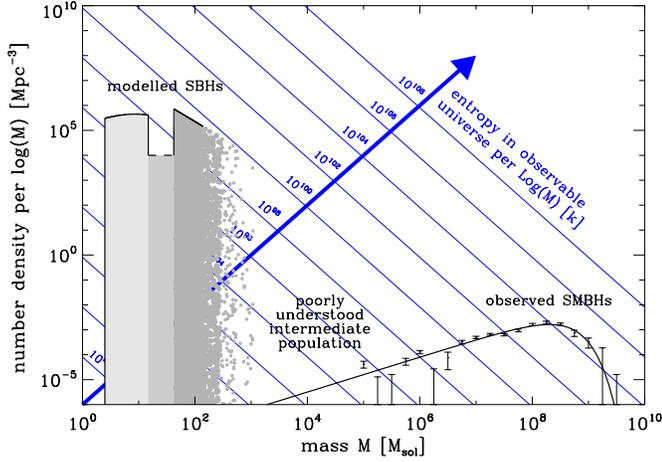$$S_{\text{SMBH}} = 3.1^{+3.0}_{-1.7} \times 10^{104}\, k. \qquad (37)$$

Figure 5. Comparing the entropic contributions of black holes of different masses. Whether or not the total black hole entropy is dominated by SMBHs depends on the yet-unquantified number of intermediate mass black holes.

(A color version of this figure is available in the online journal.)

The uncertainty here includes uncertainties in the SMBH mass function and uncertainties in the volume of the observable universe. This is at least an order of magnitude larger than previous estimates (see Table 1). The reason for the difference is that the (Graham et al. 2007) SMBH mass function contains larger black holes than assumed in previous estimates.

Frampton (2009a, 2009b) has suggested that intermediate mass black holes in galactic halos may contain more entropy than SMBHs in galactic cores. For example, according to the massive astrophysical compact halo object (MACHO) explanation of dark matter, intermediate mass black holes in the mass range 10^2–$10^5\,M_\odot$ may constitute dark matter. Assuming $10^5\,M_\odot$ black holes, these objects would contribute up to $10^{106}\,k$ to the entropy of the observable universe (Frampton 2009b). Whether or not this is so depends on the number density and mass distribution of this population. Figure 5 combines Figures 3 and 4 and shows what intermediate black hole number densities would be required.

3. THE ENTROPY OF THE COSMIC EVENT HORIZON AND ITS INTERIOR

In this section, we calculate the entropy budget for scheme 2 (refer to discussion in Section 1.1). Scheme 2 differs from scheme 1 in two ways: first, along with the components previously considered (and listed in Table 1), here we consider the CEH as an additional entropy component; and second, the volume of interest is that within the event horizon not the particle horizon (or observable universe).

The proper distance to the CEH is generally time-dependent, increasing when the universe is dominated by an energy component with an equation of state $w > -1$ (radiation and matter) and remaining constant when the universe is dark energy dominated (assuming a cosmological constant, $w = -1$). Since our universe is presently entering dark energy domination, the growth of the event horizon has slowed, and it is almost as large now as it will ever become (bottom panel of Figure 1). In the Appendix, we calculate the present radius and volume of the CEH,

$$R_{\rm CEH} = 15.7 \pm 0.4\,{\rm Glyr}, \tag{38}$$

$$\begin{aligned} V_{\rm CEH} &= 1.62 \pm 0.12 \times 10^4\,{\rm Glyr}^3 \\ &= 1.37 \pm 0.10 \times 10^{79}\,{\rm m}^3. \end{aligned} \tag{39}$$

Table 2
Entropy of the Event Horizon and the Matter Within It
(Scheme 2 Entropy Budget)

Component	Entropy S (k)
Cosmic Event Horizon	$2.6 \pm 0.3 \times 10^{122}$
SMBHs	$1.2^{+1.1}_{-0.7} \times 10^{103}$
Stellar BHs (2.5–15 $M_\odot$)	$2.2 \times 10^{96+0.6}_{\quad-1.2}$
Photons	$2.03 \pm 0.15 \times 10^{88}$
Relic Neutrinos	$1.93 \pm 0.15 \times 10^{88}$
WIMP Dark Matter	$6 \times 10^{86\pm1}$
Relic Gravitons	$2.3 \times 10^{86+0.2}_{\quad-3.1}$
ISM and IGM	$2.7 \pm 2.1 \times 10^{80}$
Stars	$3.5 \pm 1.7 \times 10^{78}$
Total	$2.6 \pm 0.3 \times 10^{122}$
Tentative Components:	
Massive Halo BHs ($10^5\,M_\odot$)	10^{104}
Stellar BHs (42–140 $M_\odot$)	$1.2 \times 10^{98+0.8}_{\quad-1.6}$

Notes. This budget is dominated by the cosmic event horizon entropy. While the CEH entropy should be considered as an additional component in scheme 2, it also corresponds to the holographic bound ('t Hooft 1993) on the possible entropy of the other components and may represent a significant overestimate. Massive halo black holes at $10^5\,M_\odot$ and stellar black holes in the range 42–140 $M_\odot$ are included tentatively since their existence is speculative.

We also calculate the present entropy of the CEH (following Gibbons & Hawking 1977),

$$\begin{aligned} S_{\rm CEH} &= \frac{kc^3}{G\hbar}\frac{A}{4} \\ &= \frac{kc^3}{G\hbar}\pi R_{\rm CEH}^2 \\ &= 2.6 \pm 0.3 \times 10^{122}\,k. \end{aligned} \tag{40}$$

Entropies of the various components within the CEH are calculated using the entropy densities s_i from Section 2:

$$S_i = s_i V_{\rm CEH}. \tag{41}$$

Table 2 shows that the cosmic event horizon contributes almost 20 orders of magnitude more entropy than the next largest contributor, supermassive black holes.

4. DISCUSSION

The second law of thermodynamics holds that the entropy of an isolated system increases or remains constant, but does not decrease. This has been applied to the large-scale universe in at least two ways (Equations (1) and (2)). The first scheme requires the entropy in a comoving volume of the universe to not decrease. The second scheme requires the entropy of matter contained within the event horizon, plus the entropy of the event horizon, to not decrease.

We have calculated improved estimates of the current entropy budget under scheme 1 (normalized to the current observable universe) and scheme 2. These are given in Tables 1 and 2, respectively.

The entropy of dark matter has not been calculated previously. We find that dark matter contributes $10^{88\pm1}\,k$ to the entropy of the observable universe. We note that the neutrino and dark matter estimates do not include an increase due to their infall
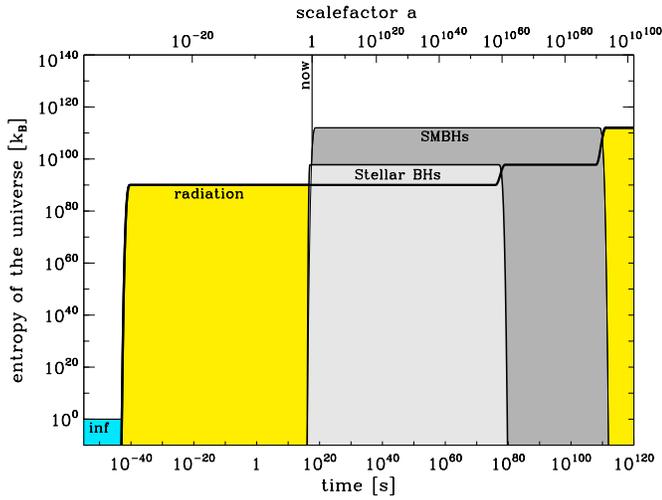
Figure 6. Entropy in a comoving volume (normalized to the present observable universe). This figure illustrates the time dependence of the scheme 1 entropy budget. N.B. $10^{10^{100}} = 1$ googolplex.

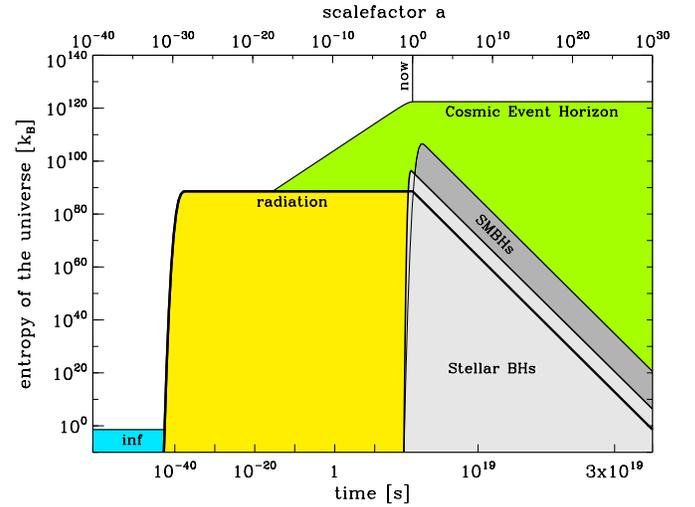(A color version of this figure is available in the online journal.)

Figure 7. Entropy of matter within the CEH, and the entropy of the CEH. This figure illustrates the time dependence of the scheme 2 entropy budget. Note: the horizontal axis is shorter than in Figure 6.

(A color version of this figure is available in the online journal.)

into gravitational potentials during structure formation. It is not clear to us a priori whether this non-inclusion is significant, but it may be since both components are presently non-relativistic. This should be investigated in future work.

Previous estimates of the relic graviton entropy have assumed that only the known particles participate in the relativistic fluid of the early universe at $t \gtrsim t_{\text{planck}}$. In terms of the number of relativistic degrees of freedom, this means $g_{*S} \rightarrow 106.75$ at high temperatures. However, additional particles are expected to exist, and thus g_{*S} is expected to become larger as $t \rightarrow t_{\text{planck}}$. In the present work, we have calculated the relic graviton entropy corresponding to three high-energy extrapolations of g_{*S} (constant, linear growth and exponential growth) and reported the corresponding graviton temperatures and entropies.

In this paper, we have computed the entropy budget of the observable universe today $S_{\text{obs}}(t = t_0)$. Figure 6 illustrates the evolution of the entropy budget under scheme 1, i.e., the entropy in a comoving volume (normalized to the current observable universe). For simplicity, we have included only the most important components.

At the far-left of the figure, we show a brief period of inflation. During this period all of the energy is in the inflaton (Guth 1981; Linde 1982), which has very few degrees of freedom and low entropy (blue fill; A. D. Linde 2009, private communication; P. Steinhardt 2009, private communication). Inflation ends with a period of reheating somewhere between the Planck scale (10^{-45} s) and the GUT scale (10^{-35} s), during which the inflaton's energy is transferred into a relativistic fluid (yellow fill). During reheating, the entropy increases by many orders of magnitude. After reheating, the constitution of the relativistic fluid continues to change, but the changes occur reversibly and do not increase the entropy.

After a few hundred million years ($\sim 10^{16}$ s), the first stars form from collapsing clouds of neutral hydrogen and helium. Shortly thereafter the first black holes form. The entropy in stellar black holes (light gray) and SMBHs (dark gray) increases rapidly during galactic evolution. The budget given in Table 1 is a snapshot of the entropies at the present time (4.3×10^{17} s). Over the next 10^{26} s, the growth of structures larger than about

$10^{14} M_\odot$ will be halted by the acceleration of the universe. Galaxies within superclusters will merge and objects in the outer limits of these objects will be ejected. The final masses of SMBHs will be $\sim 10^{10} M_\odot$ (Adams & Laughlin 1997) with the entropy dominated by those with $M \sim 10^{12} M_\odot$.

Stellar black holes will evaporate away into Hawking radiation in about 10^{80} s and SMBHs will follow in 10^{110} s. The decrease in black hole entropy is accompanied by a compensating increase in radiation entropy. The thick black line in Figure 6 represents the radiation entropy growing as black holes evaporate. The asymptotic future of the entropy budget, under scheme 1, will be radiation dominated.

Figure 7 illustrates the evolution of the entropy budget under scheme 2, i.e., the entropy within the CEH, plus the entropy of the CEH.

Whereas in scheme 1, we integrate over a constant comoving volume, here the relevant volume is the event horizon. The event horizon is discussed in some detail in the Appendix. During radiation domination, the comoving radius of the CEH is approximately constant (the proper distance grows as $R_{\text{CEH}} \propto a$); and in the dark energy dominated future, it is a constant proper distance ($R_{\text{CEH}} = \text{constant}$). The few logarithmic decades around the present time cannot be described well by either of these.

Since the event horizon has been approximately comoving in the past, the left half of Figure 7 is almost the same as in Figure 6 except that we have included the event horizon entropy (green fill). The event horizon entropy dominates this budget from about 10^{-16} s.

After dark energy domination sets in, the CEH becomes a constant proper distance. The expansion of the universe causes comoving objects to recede beyond the CEH. On average, the number of galaxies, black holes, photons, etc., within our CEH decreases as a^{-3}. The stellar and SMBH entropy contained within the CEH decreases accordingly (decreasing gray filled regions).

The decreasing black hole entropy (as well as other components not shown) is compensated by the asymptotically growing CEH entropy (demonstrated explicitly for a range of scenarios in Davis et al. 2003), and thus the second law of thermodynamics is satisfied. See C. A. Egan & C. H. Lineweaver (2010, in
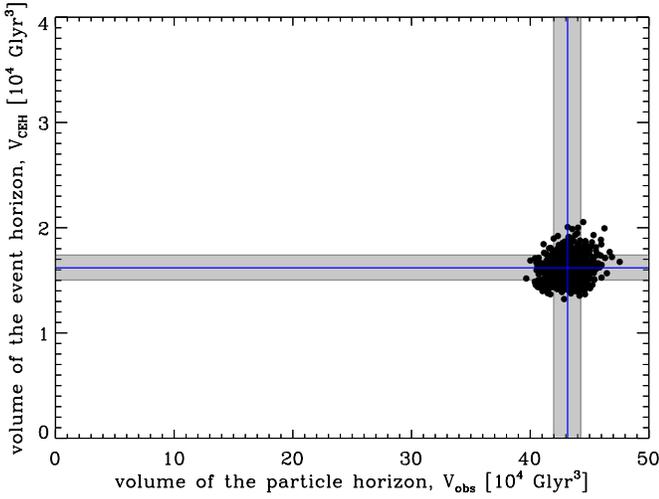
Figure 8. Eight hundred realizations of V_{obs} and V_{CEH} indicate the volume of the observable universe is $43.2 \pm 1.2 \times 10^4$ Glyr^3 (horizontal axis) and the volume of the cosmic event horizon is $V_{CEH} = 1.62 \pm 0.12 \times 10^4$ Glyr^3 (vertical axis). We note that there is only a weak correlation between uncertainties in the two volumes.

(A color version of this figure is available in the online journal.)

preparation) for further discussion of the time dependence of the entropy of the universe.

We are grateful for many useful discussions with Tamara Davis, Ken Freeman, Pat Scott, Geoff Bicknell, Mike Turner, Andrei Linde, and Paul Steinhardt. C.A.E. thanks Anna Fransson for financial support and the Research School of Astronomy and Astrophysics, Australian National University, for its hospitality during the preparation of this paper.

APPENDIX

THE OBSERVABLE UNIVERSE AND THE COSMIC EVENT HORIZON

Here we calculate the radius and volume of the observable universe (for use in Section 2); and we calculate the radius, volume, and entropy of the CEH (for use in Section 3). We use numerical methods to track the propagation of errors from the cosmological parameters.

The radius of the observable universe (or particle horizon) is

$$R_{obs} = a(t) \int_{t'=0}^{t} \frac{c}{a(t')} dt'. \tag{A1}$$

Here, $a(t)$ is the time-dependent scalefactor of the universe given by the Friedmann equation for a flat cosmology

$$\frac{da}{dt} = \sqrt{\frac{\Omega_r}{a^2} + \frac{\Omega_m}{a} + \frac{\Omega_\Lambda}{a^{-2}}}. \tag{A2}$$

Hubble's constant and the matter density parameter are taken from Seljak et al. (2006): $h = H/100 \, \text{km s}^{-1} \, \text{Mpc}^{-1} = 0.705 \pm 0.013$, $\omega_m = \Omega_m h^2 = 0.136 \pm 0.003$. The radiation density is calculated from the observed CMB temperature, $T_{CMB} = 2.725 \pm 0.002$ K (Mather et al. 1999), using $\Omega_r = \frac{8\pi G}{3H^2} \frac{\pi^2 k^4 T^4}{15 c^5 \hbar^3}$. The vacuum energy density parameter is determined by flatness, $\Omega_\Lambda = 1 - \Omega_r - \Omega_m$.

A distribution of R_{obs} values is built up by repeatedly evaluating Equation (A1) at the present time (defined by
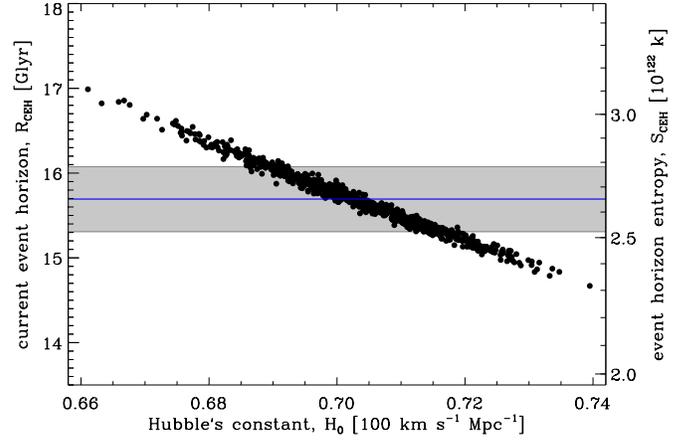

Figure 9. The radius and entropy of the cosmic event horizon. We find $S_{CEH} = 2.6 \pm 0.3 \times 10^{122} \, k$, in agreement with previous estimates $S_{CEH} \sim 10^{122} \, k$ (Bousso et al. 2007). Uncertainties in S_{CEH} come from uncertainties in R_{CEH}, which are almost exclusively due to uncertainties in h.

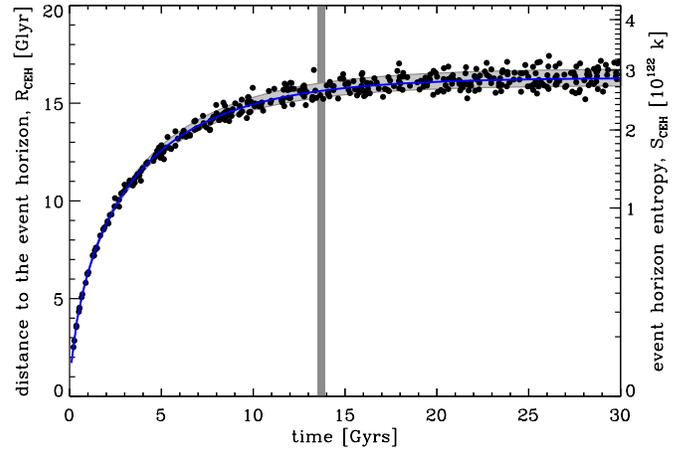(A color version of this figure is available in the online journal.)

Figure 10. Proper distance to the event horizon shown as a function of time. The vertical gray line represents the present age of the universe (and its width, the uncertainty in the present age). During dark energy domination, the proper radius, proper volume, and entropy of the CEH will monotonically increase, asymptoting to a constant.

(A color version of this figure is available in the online journal.)

$a(t_0) = 1$) using cosmological parameters randomly selected from the allowed region of $h - \omega_m - T_{CMB}$ parameter space (assuming uncorrelated Gaussian errors in these parameters). We find

$$R_{obs} = 46.9 \pm 0.4 \, \text{Glyr} \tag{A3}$$

with an approximately Gaussian distribution. The quoted confidence interval here, and elsewhere in this Appendix, is 1σ. The volume of the observable universe V_{obs} is calculated using the normal formula for the volume of a sphere.

$$V_{obs} = 43.2 \pm 1.2 \times 10^4 \, \text{Glyr}^3$$
$$= 3.65 \pm 0.10 \times 10^{80} \, \text{m}^3. \tag{A4}$$

See Figure 8. Uncertainty in R_{obs} and V_{obs} is predominantly due to uncertainty in ω_m however h also makes a non-negligible contribution.

The radius of the CEH at time t is given by integrating along a photon's world line from the time t to the infinite future.

$$R_{\mathrm{CEH}} = a(t_{\mathrm{now}}) \int_{t=t_{\mathrm{now}}}^{\infty} \frac{c}{a(t)} dt. \qquad (A5)$$

This integral is finite because the future of the universe is dark energy dominated. Using the same methods as for the observable universe, we find the present radius and volume of the CEH to be

$$R_{\mathrm{CEH}} = 15.7 \pm 0.4 \, \mathrm{Glyr}, \qquad (A6)$$

and

$$\begin{aligned} V_{\mathrm{CEH}} &= 1.62 \pm 0.12 \times 10^4 \, \mathrm{Glyr}^3, \\ &= 1.37 \pm 0.10 \times 10^{79} \, \mathrm{m}^3. \end{aligned} \qquad (A7)$$

The entropy of the CEH is calculated using the Bekenstein–Hawking horizon entropy equation as suggested by Gibbons & Hawking (1977).

$$\begin{aligned} S_{\mathrm{CEH}} &= \frac{kc^3}{G\hbar} \frac{A}{4} = \frac{kc^3}{G\hbar} \pi R_{\mathrm{CEH}}^2 \\ &= 2.6 \pm 0.3 \times 10^{122} \, k. \end{aligned} \qquad (A8)$$

Uncertainty in the CEH radius, volume, and entropy are dominated by uncertainties in Hubble's constant (Figure 9).

The CEH monotonically increases, asymptoting to a constant radius and entropy slightly larger than its current value (see Figure 10). We calculate the asymptotic radius, volume, and entropy to be

$$\begin{aligned} R_{\mathrm{CEH}}(t \to \infty) &= 16.4 \pm 0.4 \, \mathrm{Glyr} \\ &= 1.55 \pm 0.04 \times 10^{26} \, m, \end{aligned} \qquad (A9)$$

$$\begin{aligned} V_{\mathrm{CEH}}(t \to \infty) &= 1.84 \pm 0.15 \times 10^4 \, \mathrm{Glyr}^3 \\ &= 1.56 \pm 0.13 \times 10^{79} \, \mathrm{m}^3, \end{aligned} \qquad (A10)$$

$$S_{\mathrm{CEH}}(t \to \infty) = 2.88 \pm 0.16 \times 10^{122} \, k. \qquad (A11)$$

REFERENCES

Abe, S., et al. 2008, Phys. Rev. Lett., 100, 221803
Adams, F. C., & Laughlin, G. 1997, Rev. Mod. Phys., 69, 337
Adamson, P., et al. 2008, Phys. Rev. Lett., 101, 131802

Balbus, S. A., & Hawley, J. F. 2002, ApJ, 573, 749
Basu, B., & Lynden-Bell, D. 1990, QJRAS, 31, 359
Bekenstein, J. D. 1973, Phys. Rev. D, 7, 2333
Bekenstein, J. D. 1974, Phys. Rev. D, 9, 3292
Binney, J., & Tremaine, S. 2008, Galactic Dynamics (2nd ed; Princeton, NJ: Princeton Univ. Press)
Bousso, R., Harnik, R., Kribs, G. D., & Perez, G. 2007, Phys. Rev. D, 76, 043513
Cleveland, B. T., Daily, T., Davis, R. J., Distel, J. R., Lande, K., Lee, C. K., Wildenhain, P. S., & Ullman, J. 1998, ApJ, 496, 505
Coleman, T. S., & Roos, M. 2003, Phys. Rev. D, 68, 027702
Davis, T. M., Davies, P. C. W., & Lineweaver, C. H. 2003, Class. Quantum Gravity, 20, 2753
Elmegreen, B. G. 2007, in ASP Conf. Ser. 362, The Seventh Pacific Rim Conference on Stellar Astrophysics, ed. Y. W. Kang et al. (San Francisco, CA: ASP), 269
Frampton, P. H. 2009a, arXiv:0904.2934
Frampton, P. H. 2009b, J. Cosmol. Astropart. Phys., 10, 16
Frampton, P. H., Hsu, S. D. H., Kephart, T. W., & Reeb, D. 2009, Class. Quantum Gravity, 26, 145005
Frampton, P. H., & Kephart, T. W. 2008, J. Cosmol. Astropart. Phys., 6, 8
Frautschi, S. 1982, Science, 217, 593
Fryer, C. L., & Kalogera, V. 2001, ApJ, 554, 548
Fukugita, M., & Peebles, P. J. E. 2004, ApJ, 616, 643
Gibbons, G. W., & Hawking, S. W. 1977, Phys. Rev. D, 15, 2738
Gnedin, N. Y., & Gnedin, O. Y. 1998, ApJ, 509, 11
Graham, A. W., Driver, S. P., Allen, P. D., & Liske, J. 2007, MNRAS, 378, 198
Guth, A. H. 1981, Phys. Rev. D, 23, 347
Hawking, S. W. 1976, Phys. Rev. D, 13, 191
Heger, A., Woosley, S. E., & Baraffe, I. 2005, in ASP Conf. Ser. 332, The Fate of the Most Massive Stars, ed. R. Humphreys & K. Stanek (San Francisco, CA: ASP), 339
Hulse, R. A., & Taylor, J. H. 1975, ApJ, 195, L51
Kolb, E. W., & Turner, M. S. 1981, Nature, 294, 521
Kolb, E. W., & Turner, M. S. 1990, Frontiers in Physics (Reading, MA: Addison-Wesley), 1988
Linde, A. D. 1982, Phys. Lett. B, 108, 389
Lineweaver, C. H., & Egan, C. A. 2008, Phys. Life Rev., 5, 225
Lynden Bell, D. 1967, MNRAS, 136, 101
Mather, J. C., Fixsen, D. J., Shafer, R. A., Mosier, C., & Wilkinson, D. T. 1999, ApJ, 512, 511
Mather, J. C., et al. 1994, ApJ, 420, 439
Peacock, J. A. 1999, Cosmological Physics (Cambridge: Cambridge Univ. Press)
Penrose, R. 1979, in General Relativity: An Einstein Centenary Survey, ed. S. W. Hawking & W. Israel (Cambridge: Cambridge Univ. Press), 581
Penrose, R. 1987, in Three Hundred Years of Gravitation, ed. S. W. Hawking & W. Israel (Cambridge: Cambridge Univ. Press), 17
Penrose, R. (ed.) 2004, in The Road to Reality: A Complete Guide to the Laws of the Universe (London: Jonathan Cape)
Seljak, U., Slosar, A., & McDonald, P. 2006, J. Cosmol. Astropart. Phys., 10, 14
Spergel, D. N., et al. 2007, ApJS, 170, 377
Strominger, A., & Vafa, C. 1996, Phys. Lett. B, 379, 99
Susskind, L. 1995, J. Math. Phys., 36, 6377
't Hooft, G. 1993, arXiv:gr-qc/9310026
Weisberg, J. M., & Taylor, J. H. 2005, in ASP Conf. Ser. 328, Binary Radio Pulsars, ed. F. A. Rasio & I. H. Stairs (San Francisco, CA: ASP), 25